Cement & Concrete Composites 32 (2010) 571–579

Contents lists available at ScienceDirect

Cement & Concrete Composites

journal homepage: www.elsevier.com/locate/cemconcomp

Numerical modeling for predicting service life of reinforced concrete structures exposed to chloride environments

Gang Lin, Yinghua Liu *, Zhihai Xiang

Department of Engineering Mechanics, AML, Tsinghua University, Beijing 100084, China

ARTICLE INFO

Article history:
Received 10 August 2009
Received in revised form 22 June 2010
Accepted 10 July 2010
Available online 15 July 2010

Keywords:
Service life prediction
Nonsaturated concrete
Chloride environment
Diffusion–convection analysis
Thermal-hygro-mechanical model

ABSTRACT

Degradation of reinforced concrete (RC) structures due to chloride penetration followed by reinforcement corrosion has been a serious problem in civil engineering for many years. In the present paper, a systematic and robust model for predicting service life of RC structures is developed which takes environmental humidity and temperature fluctuations, chloride binding, diffusion and convection, as well as the decay of structural performance into account. The interactions between the decay of structural performance, heat and moisture transfer are considered in a coupled thermal-hygro-mechanical model. The governing equations of heat, moisture and chloride transport into nonsaturated concrete are described particularly and solved numerically by finite element analysis in space and time domains. Comparisons of numerical results with analytical solutions and experimental observations are conducted to establish the validity of the proposed numerical model. Applications of the numerical model are demonstrated by predicting service life of a RC slab exposed to a chloride environment.

1. Introduction

Chloride-induced corrosion of reinforcement has been identified as one of the most predominant degradation mechanisms in RC structures. This degradation mechanism leads to a series of structural problems, such as reduction of the cross-section area of reinforcement, cracking, spalling and delaminating of concrete cover and loss of concrete–steel bond strength, and thus reduces the load-carrying capacity of RC structures. Therefore, service life prediction of RC structures exposed to chloride environment is of great importance. A large amount of work done on service life modeling associated with chloride-induced deterioration has taken diffusion as the main transport mechanism of chloride into concrete, under the assumption that the concrete cover is fully saturated [1–5]. In reality, concrete is often found in a nonsaturated condition rather than a saturated condition, such as the case of RC structures exposed to marine environments or de-icing salts. Chloride penetration into nonsaturated concrete structures is a complex phenomenon, involving various factors such as diffusion due to non-uniform distribution of chloride ions and convection due to moisture diffusion into concrete. Saetta et al. [6] analyzed the penetration of chloride into concrete structures under combined diffusion and convection. Nielsen and Geiker [7] presented a simplified model for predicting chloride ingress into partially-saturated concrete based on Fick's second law by modifying the chloride diffusion coefficient. Ababneh et al. [8] simulated chloride penetration into nonsaturated concrete under combined mechanism of diffusion and convection by using a multiscale model. Meijers et al. [9] developed a computational model for simulating chloride ingress into nonsaturated concrete structures. Despite these efforts, some discrepancies between the predicted values and the observed data from laboratory and field still exist. This may be attributed to the particularity of this problem such as the difference of moisture transport into concrete during drying–wetting cycles, the fluctuation of external environment and the interactions between mass transport and decay of RC structural performance, etc.

The performance of concrete structures will decay gradually when exposed to multiple physical, chemical and mechanical deterioration processes. The porosity and permeability of concrete are increased due to various deterioration processes and the transport rates of various aggressive agents into concrete are accelerated accordingly. In turn, the performance of concrete structures decays further due to the accelerating deterioration processes. The coupling between mass transport and deterioration processes is becoming increasingly necessary to be considered in the durability assessment of RC structures [10]. A great deal of research has been done on modeling service life of undamaged concrete structures. Subsequently, a series of work has also been conducted to address the influence of cracking on the penetration resistance or permeability of concrete [11–14]. However, comparatively little work has been performed to quantitatively describe how these properties change when exposed to coupled deterioration processes and

* Corresponding author. Tel.: +86 10 62773751; fax: +86 10 62781824.
E-mail address: yhliu@mail.tsinghua.edu.cn (Y. Liu).

0958-9465/$ - see front matter © 2010 Elsevier Ltd. All rights reserved.
doi:10.1016/j.cemconcomp.2010.07.012

how the decay of concrete structures accelerates mass transport in concrete structures accordingly, which frequently occur in field applications.

In this paper, the interactions between the decay of structural performance, heat and moisture transfer are taken into account in a coupled thermal-hygro-mechanical model, and the alterations of porosity and permeability of concrete under the multiple coupled deterioration processes are characterized by introducing a scalar damage variable into the present model. The heat transfer, moisture transport and chloride penetration processes are formulated using the governing partial differential equations on the basis of conservation of energy and mass. A practical finite element model is built up to solve the coupled heat, moisture and chloride transfer processes in space and time domains. The numerical model is implemented and validated by comparing numerical results with analytical solutions and experimental observations. Further numerical simulations have been carried out for quantitative durability design and assessment of a RC slab exposed to a chloride environment.

vapor diffusion. Thus the moisture diffusivity during drying and wetting periods should differ [18]:

$$D_\theta = \begin{cases} D_d(\theta) = D_d^s\left\{\alpha_0 + (1-\alpha_0)\left[1+\left(\frac{1-\theta}{1-\theta_c}\right)^N\right]^{-1}\right\} & \text{during drying} \\ D_w(\theta) = D_w^0 \exp(n\theta_r) & \text{during wetting} \end{cases} \tag{3}$$

where D_d^s is the drying moisture diffusivity when totally saturated, α_0, θ_c and N are model parameters ($\alpha_0 = 0.05$, $\theta_c = 0.792$, $N = 6$ [19]); D_w^0 is the wetting moisture diffusivity at an initial water saturation degree of θ_0, n is an empirically determined constant ($n = 6$ [19]), and $\theta_r = (\theta - \theta_0)/(\theta_1 - \theta_0)$ is the normalized water saturation degree where θ_1 is the water saturation degree of totally saturated concrete. In order to reflect the dependence of moisture diffusivity D_θ on the temperature level T, the degree of hydration of concrete characterized by an equivalent hydration period t_e and the decay of concrete structures' performance characterized by a scalar damage variable d, the moisture diffusivity D_θ can be expressed as [20,21]:

$$D_\theta = \begin{cases} D_d(\theta) = D_d^s\left\{\alpha_0 + (1-\alpha_0)\left[1+\left(\frac{1-\theta}{1-\theta_c}\right)^N\right]^{-1}\right\}F_1(T)F_2(t_e)F_3(d) & \text{during drying} \\ D_w(\theta) = D_w^0 \exp(n\theta_r)F_1(T)F_2(t_e)F_3(d) & \text{during wetting} \end{cases} \tag{4}$$

2. Theoretical formulation

2.1. Heat transfer

Based on the principle of energy conservation, the heat transfer process is governed by Fourier's law as follows:

$$\mathrm{div}[\kappa \mathrm{grad}\ (T)] = \rho c \frac{\partial T}{\partial t} \tag{1}$$

where κ is the thermal conductivity of concrete (W/m K), T is the temperature of concrete (K), ρ is the density of concrete (kg/m^3), and c is the specific heat capacity of concrete (J/kg K). In the heat transfer analysis under the normal temperature environment ($263.15\ \mathrm{K} \leqslant T \leqslant 313.15\ \mathrm{K}$), κ, ρ and c vary tinily and can be assumed to be constants which have been confirmed by Martín-Pérez et al. [15] and Isgor and Razaqpur [16]. In this case, heat transfer may be solved firstly without considering the influence of other mass transport processes.

2.2. Moisture transport

Moisture transport into concrete usually involves one or a combination of transport mechanisms including water diffusion, sorptivity and permeability [17]. A complete moisture transport model should include the transfer of liquid water, vapor and air in concrete. However, in order to simplify the process and utilize the experimental data from the literature, a unified nonlinear diffusion-form equation is adopted here to describe the global moisture transport in concrete:

$$\frac{\partial(s\theta)}{\partial t} = \mathrm{div}[sD_\theta \ \mathrm{grad}\ (\theta)] \tag{2}$$

where s is the porosity of concrete, θ is the water saturation degree in the concrete pores and D_θ is the moisture diffusivity. When a partially-saturated concrete is being wet, the water is quickly absorbed through capillary suction. During dry periods, the moisture is driven out from the inside concrete by pore water evaporation as well as

where $F_1(T)$, $F_2(t_e)$ and $F_3(d)$ respectively account for the dependence of D_θ on the temperature level T, the equivalent hydration period t_e and the decay d of concrete structures' performance, and can be described as follows [20,21]:

$$F_1(T) = \exp\left[\frac{U_\theta}{R}\cdot\left(\frac{1}{T_{\mathrm{ref}}} - \frac{1}{T}\right)\right] \tag{5a}$$

$$F_2(t_e) = 0.3 + \sqrt{\frac{13}{t_e}} \tag{5b}$$

$$F_3(d) = 1 + \frac{D_{\theta,\max}}{D_{\theta,\mathrm{ref}}}\left\{1 - \left[1 + \left(\frac{d}{d_{\mathrm{cr}}}\right)^{nn}\right]^{-1}\right\} \tag{5c}$$

where U_θ is the activation energy of hydration, R is gas constant, T_{ref} is the reference temperature at which the moisture diffusivity is evaluated; t_e is an equivalent hydration period; nn and d_{cr} are model parameters ($nn = 5$, $d_{\mathrm{cr}} = 0.4$ [21]), and the value of $D_{\theta,\max}/D_{\theta,\mathrm{ref}}$ is chosen to be 20 [22].

2.3. Chloride transport

The flux $\mathbf{J}_c$ of chloride ions into saturated concrete due to diffusion is governed by Fick's first law [23]:

$$\mathbf{J}_c = -sD_c \ \mathrm{grad}\ (C_{\mathrm{fc}}) \tag{6}$$

where D_c is the effective chloride diffusion coefficient (m^2/s), C_{fc} is the concentration of chloride ions dissolved in the pore solution (kg/m^3 of pore solution).

Chloride transport in nonsaturated concrete occurs both by diffusion and convection. The flux of chloride ions due to convection can be mathematically expressed as the product of the free chloride concentration C_{fc} and the flux of moisture $\mathbf{J}_m$ [6]:

$$\mathbf{J}_c' = C_{\mathrm{fc}} \cdot \mathbf{J}_m \tag{7}$$

The total flux of chloride ions ingress into nonsaturated concrete can be obtained by combining the flux of chloride ions

due to diffusion (Eq. (6)) and the flux of chloride ions due to convection (Eq. (7)), and can be written as:

$$\mathbf{J} = -sD_c \text{ grad } (C_{fc}) - sC_{fc}\, D_\theta \text{ grad } (\theta) \tag{8}$$

Establishing chloride mass conservation results in:

$$\frac{\partial C_{tc}}{\partial t} = \frac{\partial C_{tc}}{\partial C_{fc}} \cdot \frac{\partial C_{fc}}{\partial t} = \text{div}[sD_c \cdot \text{grad } (C_{fc}) + sC_{fc}\, D_\theta \text{ grad } (\theta)] \tag{9}$$

where C_{tc} is the total chloride concentration (kg/m^3 of concrete), and $\frac{\partial C_{tc}}{\partial C_{fc}}$ represents the chloride binding capacity of concrete. The binding properties of a specific cementitious system are usually defined in the form of a binding isotherm with the amount of bound chloride C_{bc} expressed as a function of the free chloride concentration C_{fc}. The total, bound and free chloride concentrations in concrete are related by:

$$C_{tc} = C_{bc} + s\theta C_{fc} \tag{10}$$

In the present paper, Freundlich binding isotherm will be adopted to describe the relationship between bound chloride and free chloride, which can be described as follows [24]:

$$C_{bc} = \alpha C_{fc}^{\beta} \tag{11}$$

where α and β are model parameters.

To reflect the dependence of chloride diffusion coefficient D_c on the temperature level T, the age of concrete structures t, the water saturation θ and the decay of concrete structures' performance characterized by a scalar damage variable d, the effective chloride diffusion coefficient $D_{c,ref}$ of concrete, determined at some defined reference conditions, can be modified by adopting a multifactor law [6,21]:

$$D_c = D_{c,ref} \cdot f_1(T) \cdot f_2(t) \cdot f_3(\theta) \cdot f_4(d) \tag{12}$$

where $f_1(T)$, $f_2(t)$, $f_3(\theta)$ and $f_4(d)$ respectively account for the dependence of D_c on the temperature level T, the age t of concrete structures, the moisture saturation degree θ and the decay d of concrete structures' performance, and can be described as follows [6,21]:

$$f_1(T) = \exp\left[\frac{U_c}{R}\left(\frac{1}{T_{ref}} - \frac{1}{T}\right)\right] \tag{13a}$$

$$f_2(t) = \left(\frac{t_{ref}}{t}\right)^m \tag{13b}$$

$$f_3(\theta) = \theta^\eta \tag{13c}$$

$$f_4(d) = 1 + \frac{D_{c,max}}{D_{c,ref}}\left\{1 - \left[1 + \left(\frac{d}{d_{cr}}\right)^{nn}\right]^{-1}\right\} \tag{13d}$$

where U_C is the activation energy of the chloride diffusion process; t_{ref} is the time of exposure at which $D_{c,ref}$ has been measured, m is the age reduction factor; η is power index; nn and d_{cr} are model parameters ($nn = 5$, $d_{cr} = 0.4$ [21]), and the value of $D_{c,max}/D_{c,ref}$ is chosen to be 8 [25].

2.4. Decay of concrete structural performance

When exposed to various physical, chemical and mechanical deterioration processes, the performance of concrete structures decays gradually and the transport rates of various aggressive agents into concrete are accelerated accordingly. In turn, the performance of concrete structures decays further due to the accelerating deterioration processes. The interactions between mass transport and these deterioration processes are becoming increasingly necessary to be considered in durability assessment of concrete structures. Two typical deterioration processes such as heat transfer and associated thermal contraction/expansion, and moisture transfer and associated drying shrinkage/wetting expansion, which frequently occur in field applications, are taken into account herein to study the decay of performance of concrete.

In the present paper, the interactions between mass transport and the deterioration processes are taken into account in a coupled thermo-hygro-mechanical model. In this model, the coupled system of mechanical deformation, moisture transport and heat conduction is characterized by the displacement field $\mathbf{u}$, the water saturation degree θ and the temperature T together with a set of internal variables. The primary variables in the domain Ω are controlled by the balance of linear momentum, mass content and energy as:

$$\begin{aligned} &\text{div}(\boldsymbol{\sigma}) = 0 \\ &\frac{\partial(s\theta)}{\partial t} = \text{div}[D_\theta \text{ grad } (s\theta)] \\ &\rho c \frac{\partial T}{\partial t} = \text{div}[\kappa \text{ grad}(T)] \end{aligned} \tag{14}$$

The total strain of concrete structures under environment loadings can be described as follows:

$$\boldsymbol{\varepsilon}^{tot} = \boldsymbol{\varepsilon}^{me} + \boldsymbol{\varepsilon}^{th} + \boldsymbol{\varepsilon}^{sh} \tag{15}$$

where $\boldsymbol{\varepsilon}^{me}$ means mechanical strain caused by environment loadings; $\boldsymbol{\varepsilon}^{th} = \boldsymbol{\alpha}\Delta T$ is thermal strain, $\boldsymbol{\alpha} = [\alpha_T, \alpha_T, \alpha_T, 0, 0, 0]^T$ is the vector of coefficients of thermal expansion, and α_T is the thermal expansion coefficient; $\boldsymbol{\varepsilon}^{sh} = \boldsymbol{\beta}\Delta W$ is shrinkage strain, $\boldsymbol{\beta} = [\beta_{sh}, \beta_{sh}, \beta_{sh}, 0, 0, 0]^T$ is the vector of coefficients of shrinkage, $W = s\theta$ is free moisture content of concrete and β_{sh} is the shrinkage coefficient.

In the framework of concrete damage plasticity model, the evolutions of plastic strain and damage variable are usually described in an effective stress space $\bar{\boldsymbol{\sigma}}$. The effective stress $\bar{\boldsymbol{\sigma}}$ and the plastic strain can be respectively described as follows:

$$\bar{\boldsymbol{\sigma}} = \mathbf{D}_0^{el} \cdot \left(\boldsymbol{\varepsilon}^{tot} - \boldsymbol{\varepsilon}^{th} - \boldsymbol{\varepsilon}^{sh} - \boldsymbol{\varepsilon}^{pl}\right) \in \left\{\bar{\boldsymbol{\sigma}} | F(\bar{\boldsymbol{\sigma}}, \tilde{\boldsymbol{\varepsilon}}^{pl})\right\} \tag{16}$$

$$\dot{\boldsymbol{\varepsilon}}^{pl} = \dot{\lambda}\frac{\partial F^p(\bar{\boldsymbol{\sigma}})}{\partial \bar{\boldsymbol{\sigma}}} \tag{17}$$

where $\mathbf{D}_0^{el}$ is the initial elastic stiffness of concrete, F^p is the plastic potential, $\dot{\lambda}$ and F obey the Kuhn–Tucker conditions: $\dot{\lambda}F = 0, \dot{\lambda} \geqslant 0$, $F \leqslant 0$. The yield function F is used herein to account for different evolutions of strength under tension and compression in terms of effective stress [26,27]:

$$F(\bar{\boldsymbol{\sigma}}, \tilde{\boldsymbol{\varepsilon}}^{pl}) = \frac{1}{1-\alpha_p}\left(\sqrt{3\bar{J}_2} + \alpha_p \bar{I}_1 + \beta_p \langle \hat{\bar{\sigma}}_{max} \rangle\right) - \bar{\sigma}_c(\tilde{\varepsilon}_c^{pl}) \tag{18}$$

where $\bar{J}_2 = \bar{\mathbf{s}} : \bar{\mathbf{s}}/2$ is the second-invariant of the effective deviatoric stress, $\bar{\mathbf{s}} = \bar{\boldsymbol{\sigma}} - \bar{I}_1/3\mathbf{I}$, $\bar{I}_1 = \bar{\sigma}_{kk}$ is the first-invariant of the effective stress, $\hat{\bar{\sigma}}_{max}$ is the maximum principal effective stress, and the Macauley bracket $\langle \cdot \rangle$ is defined by $\langle x \rangle = \frac{1}{2}(|x| + x)$, α_p and β_p are model constants.

The relationship between Cauchy stress and effective stress can be described as follows:

$$\boldsymbol{\sigma} = (1-d)\bar{\boldsymbol{\sigma}} \tag{19}$$

The scalar damage variable d is a function of stress state and two independent uniaxial damage variables d_t and d_c, and can be described as follows:

$$1 - d = (1 - s_t d_c)(1 - s_c d_t) \tag{20}$$

where s_t and s_c are functions of stress state, and d_t and d_c are respectively the uniaxial tension and compression damage variables which are assumed to be functions of equivalent plastic strains in tension and compression, respectively [26].

3. Numerical implementation

3.1. Formulation of the present numerical model

The coupling between mass transport and various deterioration processes and the nonlinearity of material parameters involved make analytical solutions for Eqs. (14) and (9) impossible. In the present study, a finite element-based computational methodology is developed to model the coupling between mass transport process and the thermal-hydro-mechanical deterioration process. The coupled-field analysis is performed in the following manner, as illustrated in Fig. 1:

Firstly, at the beginning of each time step, temperature, water saturation degree, chloride concentration and scalar damage index are read for the next time step analysis. Secondly, the transient heat transfer analysis of concrete structures is performed and the spatial temperature distribution can be obtained accordingly. Thirdly, taking into account the dependence of moisture diffusivity on temperature, water saturation degree, equivalent hydration period and decay of concrete structures as described in Eq. (4), the coupled thermal-hygro-mechanical analysis is performed. Because of the nonlinearity of the problem, a Newton–Raphson iterative solution algorithm is adopted here to solve the nonlinear problem. When the iteration is convergent at the end of the thermal-hygro-mechanical analysis, water saturation degree and scalar damage variable at each node of the finite element model can be updated accordingly. Finally, chlorides' penetration into nonsaturated concrete under combined diffusion and convection is performed, considering the dependence of chloride diffusivity on water saturation degree, temperature, time of exposure and decay of concrete structures, as described in Eq. (12). A Newton–Raphson iteration algorithm and a successive under-relaxation method are employed to solve the diffusion–convection problem. When the iteration is convergent at the end of chlorides penetration's analysis, temperature, water saturation degree, damage index and chloride concentration at each node of the finite element model are updated accordingly and prepared for the next time step.

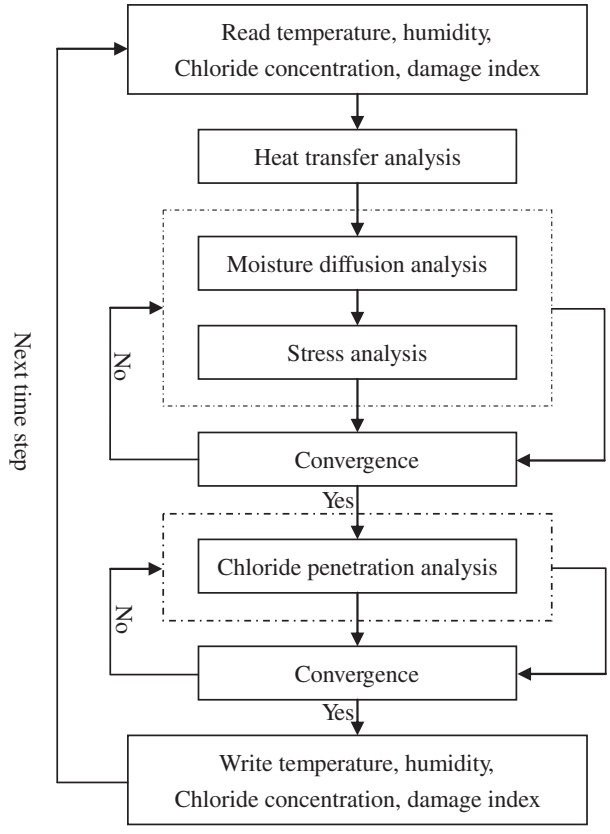

Fig. 1. Flowchart of the numerical model.

In the above analyses, the heat transfer analysis is done in ABAQUS heat transfer analysis procedure, and the coupled thermal-hygro-mechanical process is performed using the ABAQUS transient thermal-stress analysis [28]. According to Eq. (15), the equivalent thermal strain $\boldsymbol{\varepsilon}^{\mathrm{th}}_{\mathrm{eq}} = \boldsymbol{\varepsilon}^{\mathrm{th}} + \boldsymbol{\varepsilon}^{\mathrm{sh}}$ can be obtained by using ABAQUS user subroutine to define incremental thermal strains (UEXPAN). The chloride penetration into partially-saturated concrete under combined diffusion and convection is implemented by using ABAQUS user subroutine to define an element (UEL), which is described in detail in the following section.

3.2. Formulation of the UEL

The governing equation for chloride penetration into nonsaturated concrete can be expressed as follows:

$$\frac{\partial C_{\mathrm{tc}}}{\partial C_{\mathrm{fc}}}\frac{\partial C_{\mathrm{fc}}}{\partial t} = \underbrace{\mathrm{div}[sD_c\ \mathrm{grad}\ (C_{\mathrm{fc}})]}_{\text{diffusion}} + \underbrace{\mathrm{div}\ (sC_{\mathrm{fc}}D_\theta\ \mathrm{grad}\ (\theta))}_{\text{convection}} \tag{21}$$

and the boundary conditions for this problem is given as follows [6,15]:

$$J_c^s = sB_c(C_{\mathrm{en}} - C_{\mathrm{fc}}) + sC_{\mathrm{en}}B_\theta(\theta_{\mathrm{en}} - \theta) \tag{22}$$

where B_c and B_θ are respectively surface chloride and moisture transfer coefficients, C_{en} denotes the chloride concentration of environment and θ_{en} is the water saturation degree on the boundary.

Employing the Galerkin weighted residual method on the governing partial differential equation and the boundary conditions yields:

$$C_{ij}\dot{C}_{\mathrm{fc},j} + K_{ij}C_{\mathrm{fc},j} - F_i = 0 \tag{23}$$

where C_{ij}, K_{ij}, F_i are respectively the component of capacitance matrix, property matrix and load vector, and can be expressed as follow:

$$C_{ij} = \sum_e C_{ij}^e \tag{24a}$$

$$K_{ij} = \sum_e K_{ij}^e \tag{24b}$$

$$F_i = \sum_e F_i^e \tag{24c}$$

The component of element capacitance matrix C_{ij}^e, element property matrix K_{ij}^e, and element load vector F_i^e can be expressed as:

$$C_{ij}^e = \int_{\Omega_e} \frac{\partial C_{tc}}{\partial C_{fc}} N_i N_j d\Omega_e \tag{25a}$$

$$K_{ij}^e = \int_{\Omega_e} sD_c N_{i,k} N_{j,k}\, d\Omega_e - \int_{\Omega_e} sD_\theta N_i (N_{l,k}\theta_l) N_{j,k}\, d\Omega_e - \int_{\Omega_e} sN_i (N_l \dot{\theta}_l) N_j\, d\Omega_e + \int_{\Gamma_e} sB_c N_i N_j d\Gamma_e \tag{25b}$$

$$F_i^e = \int_{\Gamma_e} N_i s[B_c C_{en} + C_{en} D_\theta(\theta_{en} - \theta)] d\Gamma_e \tag{25c}$$

In Eq. (25b), k is a dummy index, (k = 1, 2 for two dimensions, while k = 1–3 for three dimensions).

Eq. (23) describes a system of first-order differential equations in the time domain. The temporal discretisation is achieved by replacing the time derivative with a finite difference approximation using the backward Euler method

$$(\mathbf{C}/\Delta t + \mathbf{K}) \cdot \mathbf{C}_{fc}^{n+1} = \mathbf{C}/\Delta t \cdot \mathbf{C}_{fc}^{n} + \mathbf{F}^{n+1} \tag{26}$$

where the superscript $(n+1)$ refers to the time level and Δt denotes a time increment. The algorithm is iterative due to the nonlinear nature of the kinetic and diffusivity. A converged solution is deemed to have achieved when:

$$\left| \frac{C_{fc,l+1}^{n+1} - C_{fc,l}^{n+1}}{C_{fc,l}^{n+1}} \right| < \delta \tag{27}$$

at all nodes where δ is a prescribed tolerance and subscript $(l+1)$ is the current iteration number.

4. Results and discussions

4.1. Comparisons with analytical results

To view the validity and accuracy of the present numerical model, we consider a transient diffusion problem and a diffusion–convection problem, respectively. The governing equations of the transient diffusion problem and the diffusion–convection problem can be respectively described as follows:

$$\text{Diffusion: } \frac{\partial C}{\partial t} = u \frac{\partial^2 C}{\partial x^2} \tag{28}$$

$$\text{Diffusion—convection: } \frac{\partial C}{\partial t} = u \frac{\partial^2 C}{\partial x^2} - v \frac{\partial C}{\partial x} \tag{29}$$

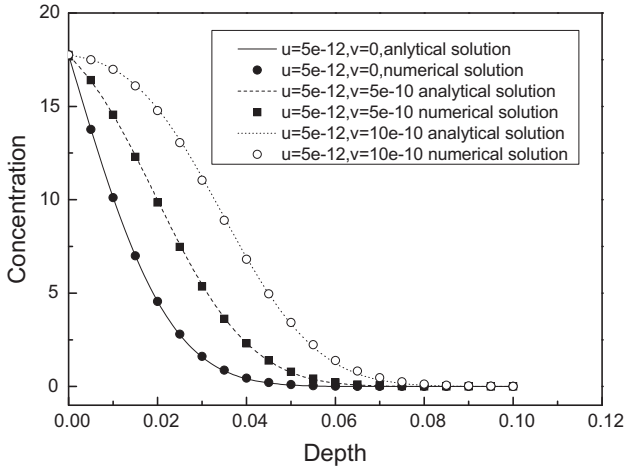

Fig. 2. Comparisons between numerical results and analytical solutions for the diffusion and convection problems.

The boundary/initial-value conditions for the diffusion and the diffusion–convection problems are given as follows:

$$\text{Boundary conditions: } C(0,t) = C_0 \quad C(\infty,t) = 0 \tag{30}$$

$$\text{Initial conditions: : } \quad C(x,0) = 0 \quad x > 0 \tag{31}$$

The analytical solutions for the diffusion problem and the diffusion–convection problem with above boundary and initial condition are respectively given as follows:

$$C(x,t) = C_0 \left[1 - \operatorname{erf}\left(\frac{x}{2\sqrt{ut}} \right) \right] \tag{32}$$

$$C(x,t) = \frac{C_0}{2} \left[\exp\left(\frac{v}{u}x\right) \operatorname{erfc}\left(\frac{x}{2\sqrt{ut}} + \frac{v\sqrt{ut}}{2u} \right) + \operatorname{erfc}\left(\frac{x}{2\sqrt{ut}} - \frac{v\sqrt{ut}}{2u} \right) \right] \tag{33}$$

The transient diffusion problem and the diffusion–convection problem are respectively solved by the present numerical model. The comparisons between analytical solutions and numerical results are illustrated in Fig. 2. The plot shows the accuracy of the numerical solution, and it can be derived that the present numerical model can be extended to more complex situations for modeling chloride penetration into nonsaturated RC structures under combined diffusion and convection.

4.2. Comparisons with experiment

In order to assess the validity of the proposed numerical model, comparisons of numerical results and experimental observations are conducted. The experimental results were obtained from the 126 days chloride penetration into concrete under different drying and wetting cycles [29]. In the experimental test, four groups of specimens (100 mm × 100 mm × 100 mm cubes) were used to simulate chloride penetration under different cyclic drying and wetting processes. All faces, except one, were protected with epoxy paint so that chloride penetration into concrete could take place through one face only. The first group was exposed to 1 mol/L NaCL solution for 126 days, while the other three groups were exposed to a series of different drying–wetting cycles, as illustrated in Fig. 3. The material properties of concrete in the experimental test are given as follows: the porosity of concrete $s = 0.161$, the chloride diffusivity $D_c = 7.92 \times 10^{-12}$ m^2/s, the moisture diffusivity during drying period $D_d^s = 1.31 \times 10^{-10}$ m^2/s, and the moisture diffusivity during wetting period $D_w^0 = 4.05 \times 10^{-11}$ m^2/s. Fig. 4 shows the comparisons of the total chloride concentration predicted by the present numerical model and those observed by experiment. It can be seen that the results predicted by the present computational framework agree well with the test data for chloride penetration into partially-saturated concrete structures under

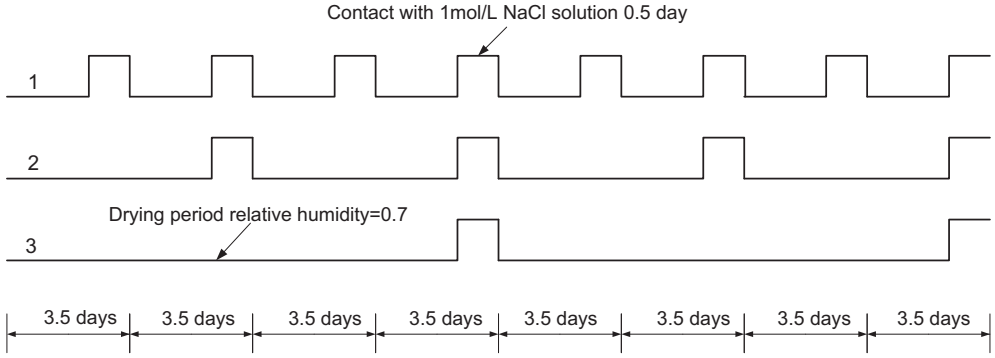

Fig. 3. Different drying–wetting periods used in the experiment.

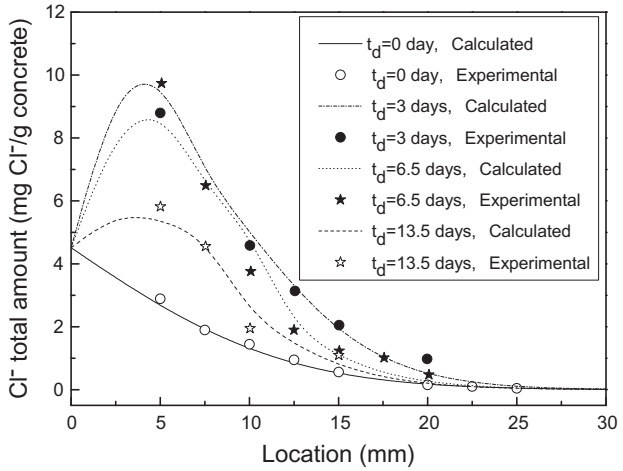

Fig. 4. Comparisons between numerical results and experimental observations under different drying–wetting periods.

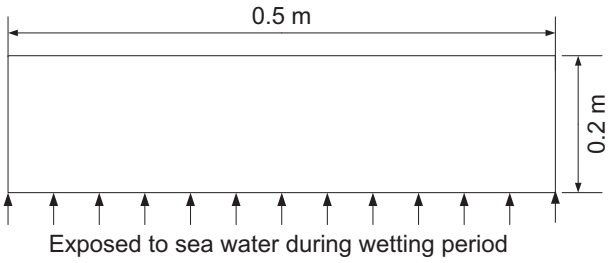

Fig. 5. Geometry of the concrete slab.

different drying and wetting cycles. The validity of the proposed implementation to model chloride ingress into partially-saturated concrete is confirmed.

4.3. Applications of the proposed numerical model

Current models for predicting the initiation time of reinforcement corrosion exposed to chloride environment are focused on chloride penetration without considering the decay of structures' performance and the difference of moisture transport during drying and wetting periods which frequently occur in field applications. In the present research, a concrete slab (length × width × height = 0.5 m × 0.2 m × 0.2 m) illustrated in Fig. 5 is selected herein to implement the simulation procedure for predicting service life of RC structure exposed to chloride environment. Only the bottom surface of the slab is exposed to sea water during the wetting period as illustrated in Fig. 6. The value of parameter C_{en}, i.e., the amount of applied chloride coming from sea water, is evaluated in the proposed numerical model by assuming a step function, wherein chloride ions are applied to the bottom surface of the specimen only during the wetting period. During the drying period, the chloride flux crossing the concrete surface is set to zero since chloride ions will remain in the concrete unless washing-away effects are taken into account. To consider the seasonal variation of ambient temperature, the annual variation of ambient temperature is assumed as a sinusoidal function as follows [6]:

$$T_{en} = 15 + 15\sin(2\pi t) \tag{34}$$

where T_{en} is the ambient temperature (°C), t is the time of exposure (years). The material properties of the concrete specimen are described in detail in Table 1.

Fig. 7 shows the free chloride profiles after an exposure period of 10 year, 30 years and 50 years, respectively. The depth of penetration is measured from the exposed surface of the concrete slab. It can be seen that the free chloride concentration reaches a maximum value about 10–15 mm inside the concrete and beyond this depth the free chloride concentration decreases with increase in the depth from the exposed surface. The variation of free chloride concentration with the time of exposure at different depth is show in Fig. 8. It is observed that, at a fixed depth inside of the concrete slab, the free chloride concentration increases with an increase in time of exposure. Service life predictions can be obtained by assuming that the service life of a RC structure exposed to chloride environment corresponds to the period until reinforcement depassivation. The free chloride threshold concentration used is 0.2% by mass of cementitious material [30]. In order to assure the initiation time of reinforcement corrosion beyond 50 years under combined deterioration process, the thickness of concrete cover should not be less than 55 mm.

In order to study the effects of convection, decay of structures and the chloride binding capacity of concrete on service life of RC structures exposed to chloride environment, comparisons of the chloride profiles predicted by the present numerical model and those predicted by these models which neglect some factors are conducted in the following.

4.3.1. Effect of convection on chloride profiles

Diffusion models are valid tools for estimating chloride profiles of concrete under saturated conditions. However, when concrete is subjected to drying–wetting environment, the transport of chloride ions due to water ingress into concrete cannot be ignored. Chloride transport in partially-saturated concrete structures is a complex phenomenon, involving various factors such as diffusion of chloride ions and movements of chlorides due to permeation of water into concrete structures. The effect of convection on chloride ingress into nonsaturated concrete plays a rather important hole. The effect of convection on the chloride profiles is researched by analyzing two different cases: the one in which chloride penetrating into concrete is driven by diffusion only, while the second one in which chloride penetrating into concrete is driven by combined diffusion and convection. The free chloride concentrations after an exposure period of 10, 30 and 50 years for the two cases are plotted in Fig. 9, respectively. It can be observed that, at any fixed depth, the free chloride concentration for the second case is much greater than that for the first case. This is due to the coupled moisture diffusion and chloride penetration, which is shown in Eq. (8). The coupling effect contributes significantly to chloride penetration into partially-saturated concrete. The variation of free chloride concentration under diffusion only with the time of exposure

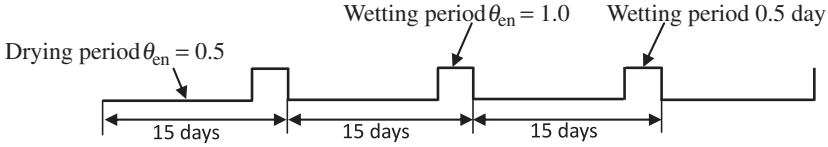

Fig. 6. Drying–wetting period.

Table 1
Values of material properties of concrete used for the numerical analysis.

Properties	Value
Porosity, s	0.10
Reference chloride diffusivity (m^2/s) $D_{c,ref}$	2.0×10^{-12}
Moisture diffusivity during drying period (m^2/s) D_d^s	2.0×10^{-10}
Moisture diffusivity during wetting period (m^2/s) D_w^0	3.22×10^{-10}
Density of concrete (kg/m^3) ρ	2400
Special heat capacity (J/kg K) c	1000
Thermal conductivity (W/m K) κ	2
Thermal expansion coefficient (1/K) α_T	1.0×10^{-5}
Shrinkage coefficient β_{sh}	9.96×10^{-3}
Environment chloride concentration (mol/L) C_{en}	0.5
Initial elastic modulus (GPa) E	27
Compression strength (MPa) f_{c0}	30
Tensile strength (MPa) f_{t0}	3.3
Dilation constant, γ_p	0.7813
Material parameters, κ_t	1.5×10^3
Material parameters, κ_c	0.5×10^3

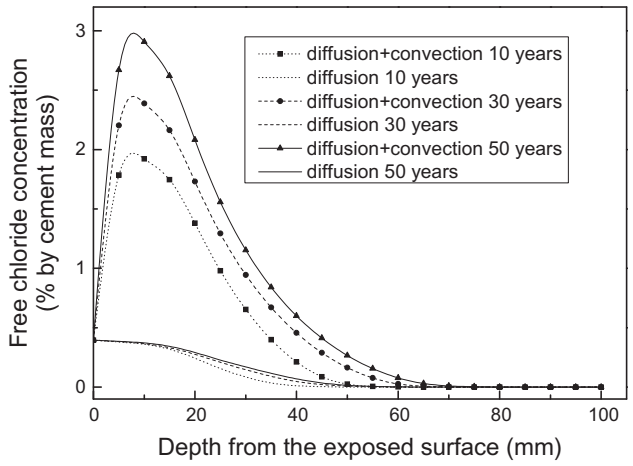

Fig. 9. Effect of convection on free chloride profiles.

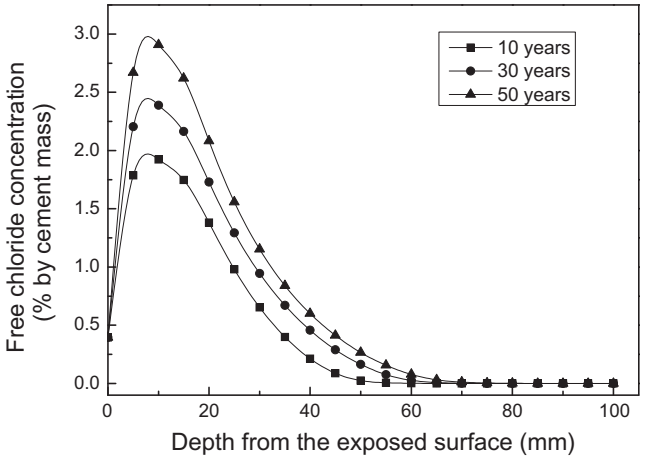

Fig. 7. Depth profile of free chloride concentration.

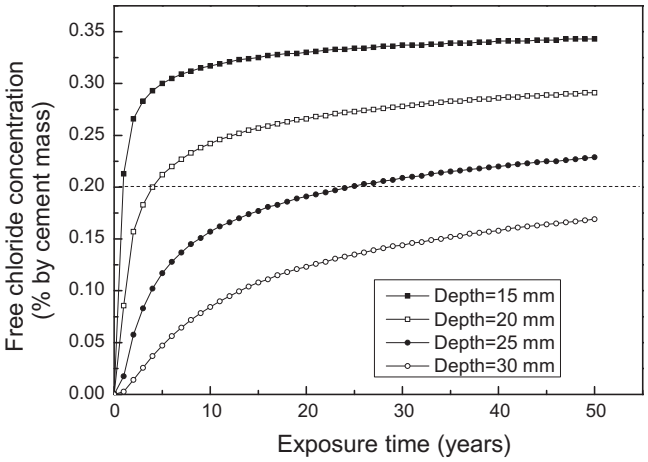

Fig. 10. Time profile of free chloride concentration when neglecting convection.

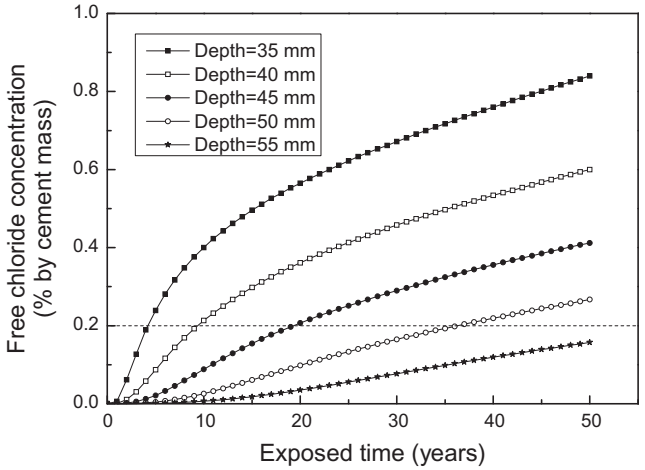

Fig. 8. Time profile of free chloride concentration.

at different depth is show in Fig. 10. It can be observed that, at a fixed depth inside of the concrete slab, the free chloride concentration increases with an increase in time of exposure. In order to assure the initiation time of reinforcement corrosion beyond 50 years under diffusion only, the thickness of concrete cover should not be less than 30 mm, as illustrated in Fig. 10, while that should not be less than 55 mm under combined diffusion and convection. It can be concluded that neglecting the effect of convection on chloride ingress into nonsaturated concrete overestimates service life of concrete structures, and this point may be essential for durability design and assessment of RC structures in the splash and tidal zones or highway concrete structures exposed to de-icing salts.

4.3.2. Effect of decay of structural performance

Most deterioration processes alter the porosity and permeability of concrete, trigger the initiation and evolution of damage, impair the durability of RC structures and thus result in accelerating aggressive agents' penetration into RC structures. In turn, the performance of concrete structures decays further due to acceleration of aggressive agents' ingress. The coupling between these deterioration processes and mass transport is becoming increasingly necessary to be considered in durability design and assessment.

The alteration of the porosity and permeability of concrete can be taken into account by introducing a scalar damage variable into the present numerical modeling. The dependence of decay of concrete structures on moisture and chloride diffusivity is taken into account by modifying the diffusivity respectively as shown Eqs. (4) and (12). The effect of decay of concrete on the chloride concentration profiles is studied by analyzing two different cases: one in

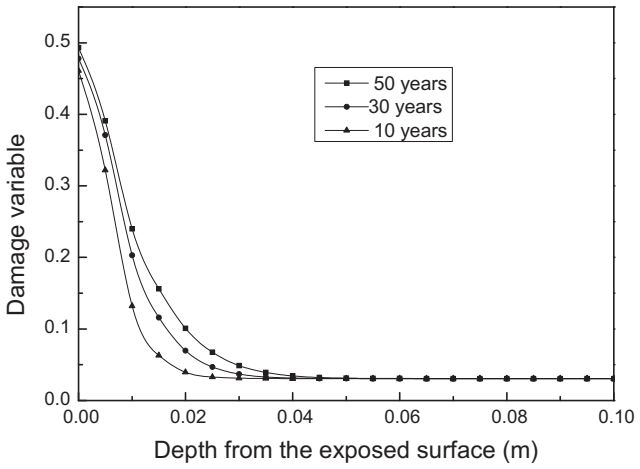

Fig. 11. Damage distribution versus time.

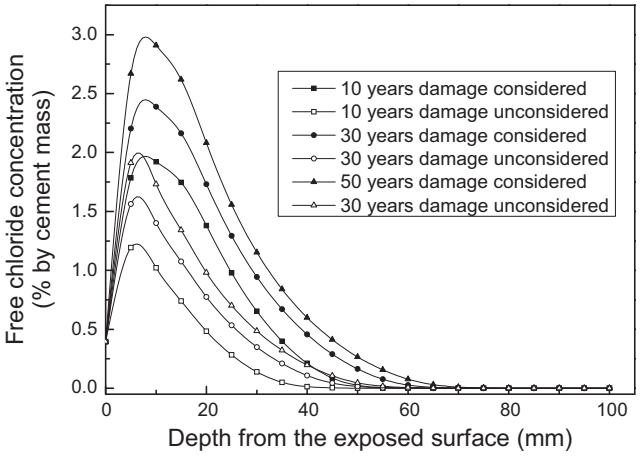

Fig. 12. Influence of damage on free chloride profiles.

which the decay of RC structures is neglected, while the other in which the decay of concrete structures is taken into account by introducing a scalar damage index. The damage variable versus time is illustrated in Fig. 11. It can be observed that the decay of the specimen is increasing due to the coupling between mass transport and various deterioration processes. The plots of free chloride concentration versus depth after 10 years, 30 years and 50 years of exposure for the two cases are shown in Fig. 12. As expected, the free concentration is higher for the second one than that for the first one. The variation of free chloride concentration in the situation of neglecting decay with the time of exposure at different depth is shown in Fig. 13. In order to assure the initiation time of reinforcement corrosion beyond 50 years, the thickness of concrete cover should not be less than 40 mm when neglecting the decay of concrete structures while that should not be less than 55 mm when taking the decay of concrete structures' durability into account.

4.3.3. Effect of binding capacity on chloride profiles

Chloride in concrete structures can be either dissolved in the pore solution (free chloride ions), or chemically and physically bound to the cement hydrates and their surfaces (bound chloride ions). Only the free chloride ions dissolved in the pore solution are responsible for initiating the process of corrosion, since the bound chloride ions are immovable and do not initiate reinforcement corrosion. However, the bound chloride ions exert a tremen-

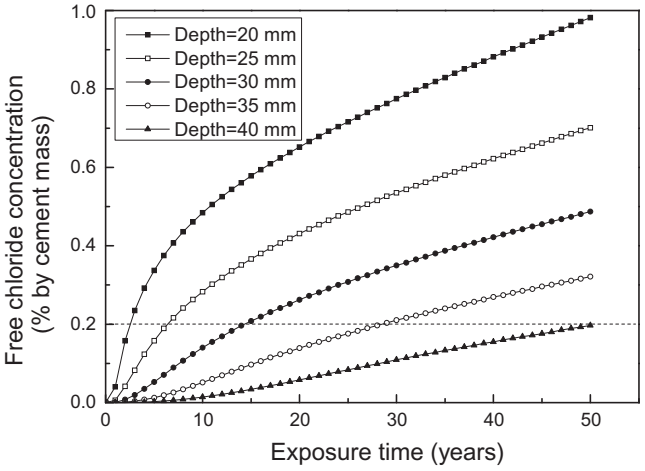

Fig. 13. Time profile of free chloride concentration when neglecting decay.

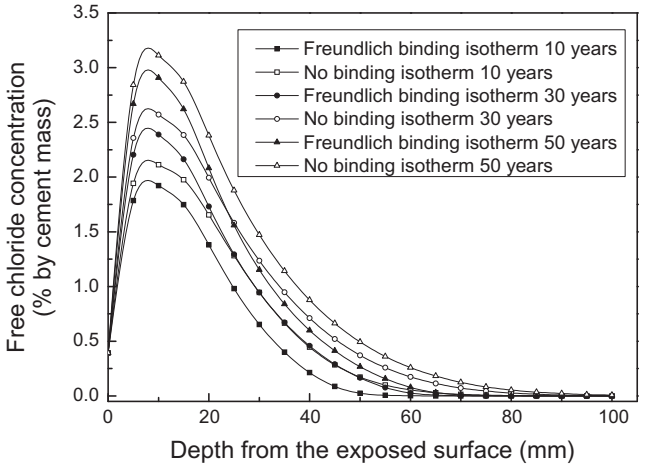

Fig. 14. Influence of binding isotherm on free chloride profiles.

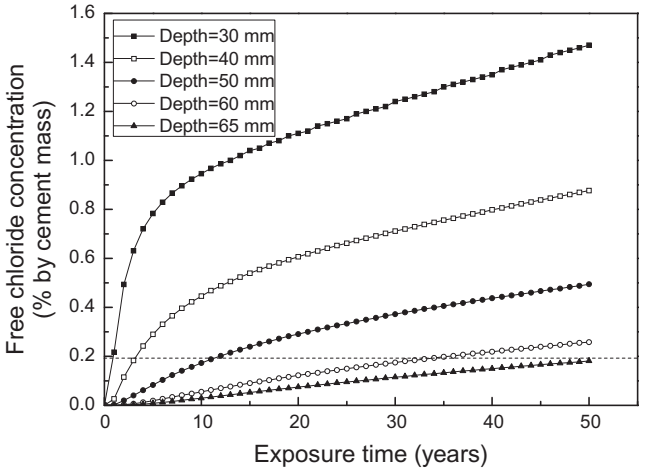

Fig. 15. Time profile of free chloride concentration when neglecting binding effect.

dous effect on free chloride ions penetration into concrete. The effect of binding isotherm nature on the chloride concentration profiles is studied by analyzing two different cases: one in which binding capacity of concrete is neglected, and the other one in which a nonlinear Freundlich binding isotherm is adopted ($\alpha = 1.037$, $\beta = 0.36$). The plots of free chloride concentration versus depth after 10, 30 and 50 years of exposure for the two cases are respectively illustrated in Fig. 14. As expected, the free chloride concentration for the first case is higher than that for the second case. It can be seen from Fig. 15 that, in order to assure the initiation time of reinforcement corrosion beyond 50 years, the thickness of concrete cover should not be less than 65 mm when neglecting binding effect, while that is should not be less than 55 mm when taking binding capacity into account. From the above analysis, it can be concluded that improving the binding chloride capacity of concrete can prolong service life of concrete structures significantly.

5. Conclusions

An integrated finite element-based numerical model has been developed in this paper for predicting service life of RC structures exposed to chloride environments, which takes environmental humidity and temperature fluctuations, chloride binding, diffusion and convection, as well as the decay of concrete structural performance into account. The interactions between mass transport and the decay of RC structures under coupled deterioration processes are considered in a coupled thermal-hygro-mechanical model. The accelerating influences of the decay of concrete durability on the transport rates of moisture and chloride are incorporated in the present model. The present study and analysis enable the following conclusions to be drawn:

(1) The difference of moisture transport into concrete during drying and wetting periods and the effect of moisture penetration on chloride ingress into partially-saturated concrete structures have been incorporated in the present numerical model. From a physical point of view, this is in better agreement with reality than the traditional models that only consider pure diffusion. It seems that in the case of a drying–wetting exposure, such as in de-icing salt environments or in the splash and tidal zones of marine concrete structures, the chloride profiles predicted by the present numerical model differ substantially from those predicted by the traditional models. This shows the need for an evaluation of service life of RC structures exposed to drying and wetting cycles on the basis of the present numerical model.

(2) When exposed to various physical, chemical and mechanical deterioration processes, the porosity and permeability of concrete structures increase gradually, and this accelerates aggressive mass into concrete structures. Therefore, neglecting the decay of concrete structural performance would overestimate service life of concrete structures.

(3) The binding capacity of concrete exerts a tremendous influence on chloride ingress into concrete structures, and this would reduce free chloride concentration near the reinforcement and could prolong concrete structures' service life. Consequently, improving chloride binding capacity of concrete can extend service life of RC structures exposed to chloride environment.

Acknowledgements

This work was a part of a project on service life modeling of concrete structures, which was funded by the Ministry of Transport of the People's Republic of China (No. 20060885). The authors are grateful for this financial support.

References

[1] Sergi G, Yu S, Page C. Diffusion of chloride and hydroxyl ions in cementitious materials exposed to a saline environment. Mag Concr Res 1992;44(158):63–9.
[2] Masi M, Colella D, Radaelli G, Bertolini L. Simulation of chloride penetration in cement-based materials. Cem Concr Res 1997;27(10):1591–601.
[3] Khatri RP, Sirivivatnanon V. Characteristic service life for concrete exposed to marine environments. Cem Concr Res 2004;34(5):745–52.
[4] Song HW, Shim HB, Petcherdchoo A, Park SK. Service life prediction of repaired concrete structures under chloride environment using finite difference method. Cem Concr Compos 2009;31(2):120–7.
[5] Marchand J, Samson E. Predicting the service-life of concrete structures – limitations of simplified models. Cem Concr Compos 2009;31(8):515–21.
[6] Saetta AV, Scotta RV, Vitaliani RV. Analysis of chloride diffusion into partially saturated concrete. ACI Mater J 1993;90(5):441–51.
[7] Nielsen EP, Geiker MR. Chloride diffusion in partially saturated cementitious material. Cem Concr Res 2003;33(1):133–8.
[8] Ababneh A, Benboudjema F, Xi Y. Chloride penetration in nonsaturated concrete. J Mater Civil Eng 2003;15(2):183–91.
[9] Meijers SJH, Bijen JMJM, Borst RD, Fraaij ALA. Computational results of a model for chloride ingress in concrete including convection, drying–wetting cycles and carbonation. Mater Struct 2005;38(2):145–54.
[10] Chen D, Mahadevan S. Cracking analysis of plain concrete under coupled heat transfer and moisture transport processes. J Struct Eng – ASCE 2007;133(3):400–10.
[11] Francois R, Maso JC. Effect of damage in reinforced concrete on carbonation or chloride penetration. Cem Concr Res 1988;18(6):961–70.
[12] Samaha HR, Hover KC. Influence of microcracking on the mass transport properties of concrete. ACI Mater J 1992;89(4):416–24.
[13] Aldea CM, Shah SP, Karr A. Effect of cracking on water and chloride permeability of concrete. J Mater Civil Eng 1999;11(3):181–7.
[14] Lim CC, Gowripalan N, Sirivivatnanon V. Microcracking and chloride permeability of concrete under uniaxial compression. Cem Concr Compos 2000;22(5):353–60.
[15] Martín-Pérez B, Pantazopoulou SJ, Thomas MDA. Numerical solution of mass transport equations in concrete structures. Comput Struct 2001;79(13):1251–64.
[16] Isgor OB, Razaqpur AG. Finite element modeling of coupled heat transfer, moisture transport and carbonation processes in concrete structures. Cem Concr Compos 2004;26(1):57–73.
[17] Li KF, Li CQ, Chen ZY. Influential depth of moisture transport in concrete subject to drying–wetting cycles. Cem Concr Compos 2009;31(10):693–8.
[18] Janssen H, Blocken B, Carmeliet J. Conservative modelling of the moisture and heat transfer in building components under atmospheric excitation. Int J Heat Mass Transfer 2007;50(5–6):1128–40.
[19] Wong SF, Wee TH, Swaddiwudhipong S, Lee SL. Study of water movement in concrete. Mag Concr Res 2001;53(3):205–20.
[20] Bazant ZP, Najjar LJ. Nonlinear water diffusion in nonsaturated concrete. Mater Struct 1972;5(1):3–20.
[21] Gerard B, Pijaudier-Cabot G, Laborderie C. Coupled diffusion-damage modelling and the implications on failure due to strain localisation. Int J Solids Struct 1998;35(31–32):4107–20.
[22] Cerny R, Drchalova J, Rovnanikova P. The effects of thermal load and frost cycles on the water transport in two high-performance concretes. Cem Concr Res 2001;31(8):1129–40.
[23] Crank J. The mathematics of diffusion. London: Oxford Univ. Press; 1975.
[24] Tang L, Nilsson LO. Chloride binding capacity and binding isotherms of OPC pastes and mortars. Cem Concr Res 1993;23(2):247–53.
[25] Gerard B, Marchand J. Influence of cracking on the diffusion properties of cement-based materials: Part I: Influence of continuous cracks on the steady-state regime. Cem Concr Res 2000;30(1):37–43.
[26] Lee JH, Fenves GL. Plastic-damage model for cyclic loading of concrete structures. J Eng Mech – ASCE 1998;124(8):892–900.
[27] Cicekli U, Voyiadjis GZ, Abu Al-Rub RK. A plasticity and anisotropic damage model for plain concrete. Int J Plast 2007;23(10–11):1874–900.
[28] ABAQUS version 6.5. Hibbitt, Karlsson and Sorensen Inc., Pawtucket; 2004.
[29] Li CQ. Water and ionic transport processes in cover concrete under drying–wetting cycles. PhD thesis. Beijing (China), Tsinghua University; 2009.
[30] American Concrete Institute. Corrosion of metals in concrete. ACI manual of concrete practice. ACI Committee 222R-01; 2002.